Influence of the composition of natural gas-hydrogen blends (HCNG) on performance and CO_2 emissions of a spark ignition engine

Emilio Navarro*
Dept. Motopropulsión y Termofluidodinámica, E.T.S.I. Aeronáuticos
Universidad Politécnica de Madrid, Madrid, Spain
E–mail: emilio.navarro@upm.es

Teresa J. Leo, Roberto Corral
Dept. Sistemas Oceánicos y Navales, E.T.S.I. Navales
Universidad Politécnica de Madrid, Madrid, Spain
E–mail: teresa.leo.mena@upm.es

ABSTRACT

Addition of hydrogen to natural gas could be a short-term alternative to nowadays fossil fuels as the emissions of greenhouse gases may be reduced. The aim of this study is to evaluate the performance and emissions of a spark ignition engine fuelled with pure natural gas, pure hydrogen and different blends of hydrogen and natural gas (HCNG). The increase of the hydrogen fraction leads to variations in the cylinder pressure and CO_2 emissions. In this work, a combustion model based on thermodynamic equations is used considering separated zones for the burned and unburned gases. The results show that the maximum cylinder pressure gets higher as the fraction of hydrogen in the blend increases. The presence of hydrogen in the blend leads to a decrease in the CO_2 emissions. Due to hydrogen properties, leaner fuel-air mixtures can be used along with the appropriate spark timing, leading to an engine emissions improvement without a performance worsening.

INTRODUCTION

Crude oil reserves are not unlimited. In the future, this will compel to resort oil fields much more difficult to exploit (higher depths, higher densities) and additional extraction problems will arise. These circumstances will probably oblige to invest in more developed extraction techniques, thus leading to an increase of the crude price. In addition, it is important to note that demand increase is higher than the supply one, becoming more evident with the development of new economies like China or India, which will require big amounts of energy supply.

On the other hand, the growing environmental concern in all fields of knowledge also affects the engine manufacturing industry. In order to be more environmental friendly, the studies focus on decreasing the emissions of greenhouse gases to the atmosphere and developing different alternatives to fossil fuels.

Natural gas is considered as an adequate alternative fuel because, compared with other fossil fuels, its combustion features are cleaner and higher proven reserves are available [1, 2], see Figure 1. Natural gas has excellent anti-knock properties, being the compression ratio higher, thus improving efficiency and power. However its flame propagation rate is low and the auto ignition temperature is high.

* Corresponding author

Hydrogen is postulated as the long-term alternative as, although not free, it is abundant in nature and the combustion products are almost harmless. However, nowadays most of the hydrogen is obtained via fossil fuels, without solving the dependency on these fuels. Moreover, hydrogen storage is also a big issue because it is very explosive, and the size and weight of the deposits are high. Hydrogen has high flame propagation rates, therefore it is easier to ignite and the engine's performance is reduced comparing to fossil fuels.

An alternative solution as transition to hydrogen technology is natural gas blended with hydrogen, known as HCNG. A combination of the two fuels could solve the limitations of both pure natural gas and hydrogen.

When experimental or simulation studies on reciprocating engines are carried out, much attention is paid to pollutant CO, HC and NO_x emissions. Nevertheless, although one of the most important gases with greenhouse effect is CO_2, these emissions are not usually taken into account and either measurements or calculations of them are obviated in many studies. This is the case of HCNG mixtures studies, where only a few analyze CO_2 emissions. Thus, experimental tests are performed in [3] to validate the proposed model, but no other studies are made; the authors in [4] use a model to study NO_x variation with 0%, 5%, 10% and 15% of H_2 in the mixtures; those in [5] carry out a thermodynamic analysis where CO and NO_x emissions are analyzed with 0%, 10% and 15% H_2 mixtures; tests with mixtures containing 0% and 29% of H_2 are performed in [6] and HC and NO_x emissions are registered; a quasi-dimensional model, with mixtures containing 0%, 50% and 100% of H_2, is used in [7] to study CO and NO emissions; the tests performed in [8] with a supercharged engine contain mixtures with 0%, 30% and 55% of H_2 reporting only CO, HC and NO_x emissions, and an experimental study [9] on 0%, 5%, 10% and 15% of H_2 mixtures determines CO, HC and NO_x.

It is just recently when experimental studies reporting CO_2 emissions data are being published. Thus, in [10] and [11] CO_2 emissions from 0%, 10%, 20%, 30% and 40% H_2 in mixtures are also determined; in [12] CO_2 emissions data are given for mixtures with a H_2 content of 0%, 15%, 20% and 25%; the authors in [13] and [14] determine CO_2 with H_2 0%, 10%, 20% and 30% mixtures whereas CO_2 from 30% H_2 mixtures is reported in [15]. These works show that emissions of hydrocarbons (HC), CO and CO_2 decrease significantly when hydrogen is used rather than pure natural gas. By using lean mixtures and optimizing spark timing, emissions can be lower.

Therefore it is worthwhile to pay attention to CO_2 emissions, and to perform a quantitative study on the influence of hydrogen amount present in a HCNG mixture. This has been considered as a very interesting topic. As the studies found in the literature practically cover the 0% - 30% H_2 range, a wider one would result quite useful to discuss the engine's performance.

With these aims, in the present study, a model of the engine cycle variations of a spark ignition engine fuelled with hydrogen-natural gas blends has been developed in order to analyse the influence of the hydrogen fraction on the engine's performance and CO_2 emissions. NO_x emissions are not presented because the kinetic of the combustion has not been considered, and most of the NO_x is produced through the oxidation of nitrogen formed in the combustion process.

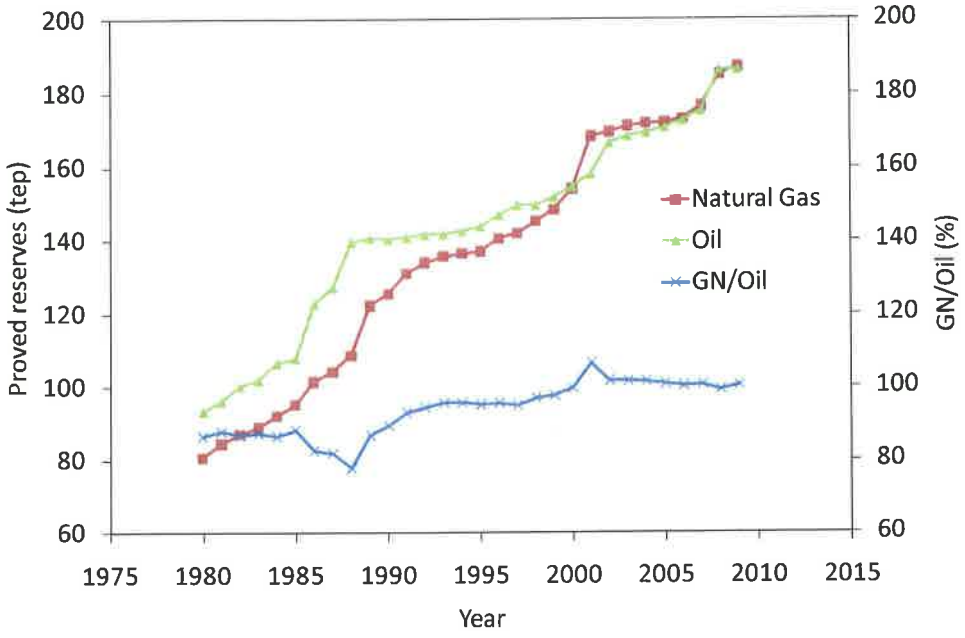

Figure 1. Proved oil and natural gas reserves

NATURAL GAS

Regarding emissions, natural gas is one of the cleaner fossil fuels existing nowadays. Therefore natural gas is one of the alternatives under study in order to accomplish oil substitution. Nevertheless, certain properties of natural gas make spark ignition engines operation difficult. Its low flame propagation speed during combustion represents the main difficulty. This may be overcome through the spark timing optimization, by the combustion chamber design improvement or by a turbulence increment.

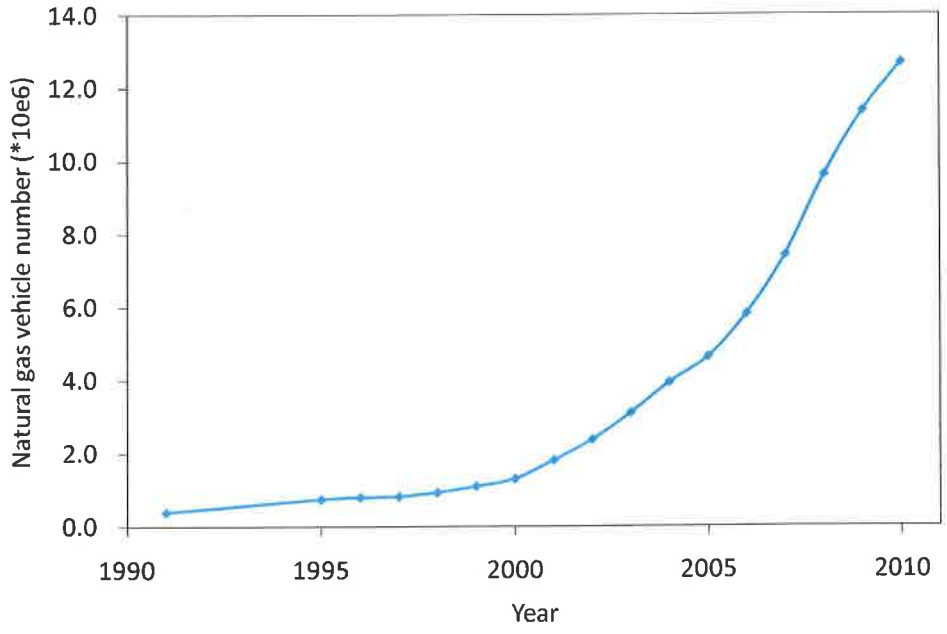

Figure 2. Total natural gas vehicles number

The interest on this fuel can be evidenced by the prediction about manufactured serial vehicles increment utilizing this fuel [16], Figure 2. Major increments are located in Western Europe and Asia. In addition, it is interesting to take into account the purchase cost increment of a vehicle using natural gas comparing to those equipped with conventional engines. Figure 3 [17, 18] shows a cost increment between 10.1% and 13.2% regarding a vehicle equipped with a gasoline spark ignition engine with injection in the intake manifold. Estimates have been made assuming vehicle production-line assembly.

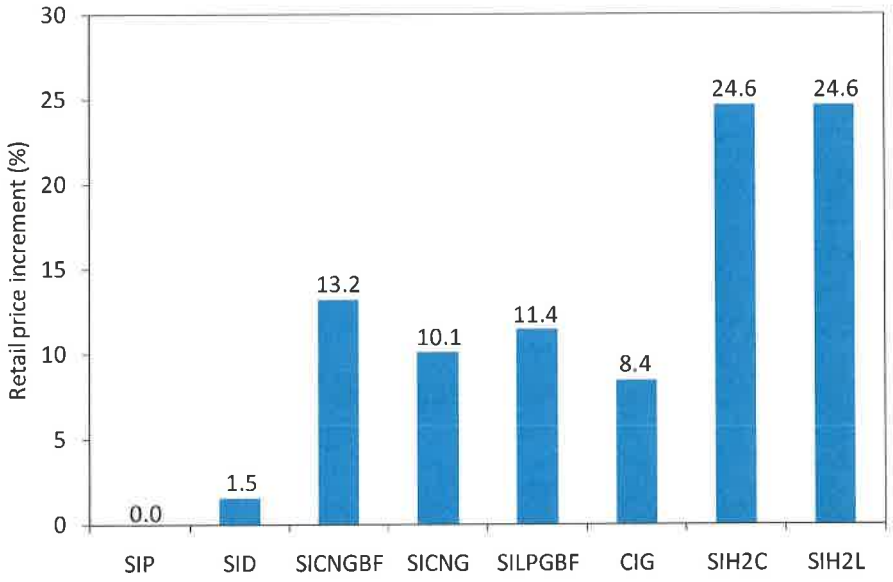

Figure 3. Incremental vehicle retail price compared to the gasoline engine using the Port Injection Spark Ignition (SIP) technology (see the Nomenclature Section for the full meaning of the abbreviations used)

Fuel costs and their relation with equivalent CO_2 emissions are represented in Figure 4 for several fuels.

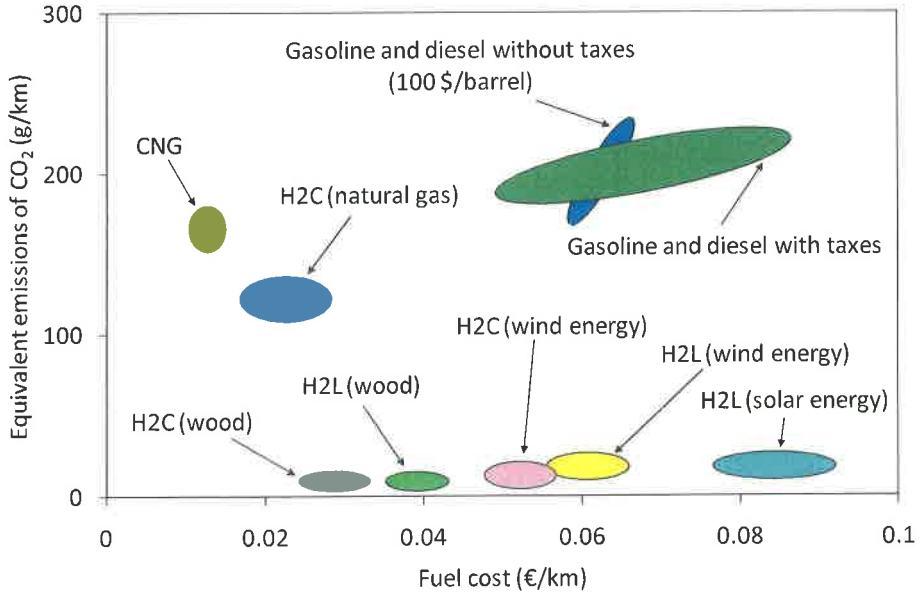

Figure 4. Cost and CO_2 emissions for several fuels

As observed, global CO_2 emissions associated to CNG and its cost are lower than those produced by gasoline or diesel. Hydrogen produces lower CO_2 emissions, although wide variations are present depending on its origin. A wide cost range is also found, capable of being reduced through mass production.

ENGINE CYCLE SIMULATION

Among the possible indicated cycle simulation models, a zero-dimensional one has been chosen to be developed. It involves two regions at the combustion stage, unburned and burned gases. The reason for that selection is based on the aim of this work: to perform various engines' parametric and optimization studies as a previous phase to the development or modification process to make the engine able to operate with HCNG mixtures. Thus, it is important to avoid a number of details to be changed later, like the combustion chamber geometry.

The used model requires less fitting parameters than others more complex but, in this case, this will not lead to worse results. For example, those models using a turbulent combustion scheme to determine the burned mass fraction, usually based on [19], require a great number of fitting parameters. When adopting literature values instead of performing the fitting process,, the uncertainty in the obtained results increases. Beside, the combustion chamber geometry must be known in order to determine the front flame location and geometry by means of procedures like the ones proposed in [20, 21].

In the zero-dimensional model with two zones, each of these regions can be studied separately as two systems with uniform composition and thermodynamic state. The geometry calculation of both regions is required to evaluate the heat transfer [22 - 25]. Models assuming similar hypotheses have been developed to study the behaviour of reciprocating engines with diverse pure fuels [26]. In this work, the fuel consists of a natural gas and hydrogen mixture at variable proportions.

To develop the model proposed [27], the following assumptions and approximations are considered:

1. The fluid under study behaves as an ideal mixture constituted by:
   a. Humid air, fuel and residual gases, during the intake and compression processes.
   b. Two regions, one corresponding to the unburned mixture (air, fuel and residual gases) and the other to the burned gases, during the combustion process.
   c. The combustion products, during the expansion process.
2. The fluid velocity inside the combustion chamber is negligible.
3. The blow-by effect is neglected.
4. Spherical front flame is assumed.
5. Uniform temperature is assumed in each region.
6. Unburned gas properties determination is performed by neglecting the pre-flame reactions, assuming the gas is frozen (the gas consists of a mixture of ideal gases).
7. Local thermodynamic equilibrium is assumed, allowing the use of the ideal gas state equation with the burned and unburned gas [28].
8. The reactant gas mixture is at thermodynamic equilibrium.

Mixing and intake processes

The fuel is introduced in the intake manifold and mixed with air. The chemical equation of the process is

$$\varepsilon\cdot\phi\left(\nu_1 CH_4(g)+\nu_2 H_2(g)\right)_{(T_f,p_f)}+\left(0.21O_2+0.79N_2+\tilde{\omega}H_2O\right)_{(T_i,p_i)}\rightarrow \left(0.21O_2+0.79N_2+\tilde{\omega}H_2O\right)_{(T,p)}+\varepsilon\cdot\phi\cdot\left(\nu_1 CH_4(g)+\nu_2 H_2(g)\right)_{(T,p)} \quad (1)$$

where ε is the total mole number of fuel, ϕ represents the fuel/air equivalence ratio, $\tilde{\omega}$ represents the molar humidity ratio and ν_i stands for the mole amount of component i per mole of fuel mixture. If pure gas natural is used $\nu_2 = 0$, but $\nu_1 = 0$ if pure hydrogen is used.

Thermodynamic properties of the obtained air-fuel mixture are calculated by means of the First Law of Thermodynamics applied to the mixing process. Variations of kinetic and potential energies have been neglected and no work is assumed during the process. The resulting equation to solve is

$$\sum_{n=1}^{N}\varepsilon\cdot\phi\cdot\nu_i\left[\int_{T_0}^{T}c_{p_i}^{o}(T)dT-\int_{T_0}^{T_f}c_{p_i}^{o}(T)dT\right]+0.21\left[\int_{T_0}^{T}c_{p_{O_2}}^{o}(T)dT-\int_{T_0}^{T_i}c_{p_{O_2}}^{o}(T)dT\right]+ +0.79\left[\int_{T_0}^{T}c_{p_{N_2}}^{o}(T)dT-\int_{T_0}^{T_i}c_{p_{N_2}}^{o}(T)dT\right]+\tilde{\omega}\left[\int_{T_0}^{T}c_{p_{H_2O}}^{o}(T)dT-\int_{T_0}^{T_i}c_{p_{H_2O}}^{o}(T)dT\right]-Q=0 \quad (2)$$

where $c_{p_i}^{0}$ represents the constant pressure specific thermal capacity of gas i, considered as an ideal gas [29], T_0 stands for the reference temperature (298.15 K), T_i is the intake air temperature and T_f represents the fuel temperature previously to its injection, and Q is the heat transfer during the process.

Once the air-fuel mixture is obtained, it is introduced into the cylinder. This phase is characterized by the mixing process of the residual gases inside the cylinder after the exhaust phase and the fuel-air mixture entering the cylinder.

To calculate the thermodynamic conditions during the gas exchange processes, the general equation to solve is

$$\frac{dp_c}{dt}=\gamma_c p_c\left(\frac{\dot{m}_i}{m_c}\frac{\Delta h_i}{c_{p,c}T_c}-\frac{\dot{m}_e}{m_c}\frac{\Delta h_e}{c_{p,c}T_c}-\frac{\dot{V}_c}{V_c}\right)+\frac{dm_c}{dt}\frac{(c_{p,c}T_c-\Delta h_c)}{V_c}(\gamma_c-1)-\frac{\dot{Q}}{V_c}(\gamma_c-1) \quad (3)$$

where e stands for exhaust and i means intake. In this equation γ_c, $c_{p,c}$ and V_c represent thermal capacity ratio, constant pressure specific thermal capacity and volume of the cylinder, respectively, $\dot{m}$ means mass flow rate and $\dot{Q}$ stands for the heat transfer rate. In addition, the following equations must be used

$$\frac{dm_c}{dt}=\dot{m}_i-\dot{m}_e \quad (4)$$

and

$$\dot{m}=\begin{cases} c_D A_s \dfrac{p_t}{\sqrt{R_g \cdot T_t}}\left(\dfrac{p_s}{p_t}\right)^{\frac{1}{\gamma}}\sqrt{\dfrac{2\gamma}{\gamma-1}\left[1-\left(\dfrac{p_s}{p_t}\right)^{\frac{\gamma-1}{\gamma}}\right]} & , \text{ if } \dfrac{p_t}{p_s}<\left(\dfrac{\gamma+1}{2}\right)^{\frac{\gamma}{\gamma-1}} \\ c_D A_s \dfrac{p_t}{\sqrt{R_g \cdot T_t}}\sqrt{\gamma}\left(\dfrac{2}{\gamma+1}\right)^{\frac{\gamma+1}{2(\gamma-1)}} & , \text{ if } \dfrac{p_t}{p_s}\geq\left(\dfrac{\gamma+1}{2}\right)^{\frac{\gamma}{\gamma-1}} \end{cases} \tag{5}$$

where c_D is the discharge coefficient, A_s represents the throat area, and p_t and p_s stand for the stagnation pressure and the pressure at the throat, respectively.

Besides, to evaluate the heat transfer rate, calculation of the convection heat transfer coefficient is required. Therefore, similarly to the compression process detailed in the following section, the Woschni [30] equation is used (equations (11) and (12) and Table 1).

Compression and expansion

For both the compression and expansion phases, the equations governing such processes are similar, exception made that the gas composition during the expansion process is variable due to the existence of dissociation reactions.

Thermodynamic conditions during the process are determined by means of the First Law of Thermodynamics applied to the fluid inside the cylinder. Variations of mechanical energy are neglected and the ideal gas state equation is used for the gas mixture. Then, dividing by the crank angle θ, the following expression can be written

$$\frac{dp}{d\theta}=-\gamma\frac{p}{V}\frac{dV}{d\theta}+\frac{\gamma-1}{V}\frac{dQ}{d\theta} \tag{6}$$

The terms appearing in this equation are evaluated by means of the following expressions

$$\frac{dQ}{d\theta}=\frac{h(\theta)A(\theta)(T(\theta)-T_w)}{n} \tag{7}$$

where h and n stand for the convection heat-transfer coefficient and the crankshaft rotational speed, respectively. The wall temperature is represented by T_w. The total area A is the sum of the cylinder liner A_c, cylinder head A_{ch} and piston crown A_p surface areas, respectively

$$A=A_c+A_{ch}+A_p=\pi Dy+\frac{\pi D^2}{2} \tag{8}$$

which can be expressed as a function of the cylinder bore D and the instantaneous stroke y. This magnitude can be calculated by

$$y=h_{cc}+a\left[\sqrt{(2\lambda+1)^2-e^2}-\cos\theta-\sqrt{4\lambda^2-(\sin\theta-e)^2}\right] \tag{9}$$

being h_{cc} the equivalent height of the combustion chamber, and a, λ and e represent the crank radius, the ratio of connecting rod length to crank radius and the relative offset (cylinder axis offset from the crankshaft axis/radius of crank), respectively

$$h_{cc} = \frac{L}{r_c - 1} = \frac{a\left[\sqrt{(2\lambda+1)^2 - e^2} - \sqrt{(2\lambda-1)^2 - e^2}\right]}{r_c - 1} \tag{10}$$

where r_c stands for the compression ratio and L is the piston stroke.

As said above, the convection heat transfer coefficient is calculated by the Woschni equation

$$h = CD^{m-1} p^m T^{0.75-1.62m} U^m \tag{11}$$

where

$$U = C_1 S_p + C_2 \frac{V_d T_r}{p_r V_r}(p - p_m) \tag{12}$$

being S_p the mean piston velocity, V_d the displaced cylinder volume, p_m the motored cylinder pressure and T_r, p_r and V_r represent inlet valve closing temperature, pressure and volume, respectively.

Table 1. Woschni coefficients

	Gas exchange	Compression	Combustion and expansion
C	3.26	3.26	3.26
m	0.8	0.8	0.8
C_1	6.18	2.28	2.28
C_2	0	0	$3.24\ 10^{-3}$

The wall temperature is evaluated by means of [31]

$$T_w = 440 + 9\eta_{vg}(nD)^{0.2} \tag{13}$$

with η_{vg} being the volumetric efficiency.

Afterwards, equations (6) to (13) lead to

$$\frac{dp}{d\theta} = -\gamma \frac{p}{V}\frac{dV}{d\theta} + \\ + \frac{\gamma - 1}{nV}\left[CD^{m-1} p^m T^{0.75-1.62m}\left(C_1 S_p + C_2 \frac{V_d T_r}{p_r V_r}(p - p_m)\right)^m \left(\pi Dy + \frac{\pi D^2}{2}\right)\left[T - \left(440 + 9\eta_{vg}(nD)^{0.2}\right)\right]\right] \tag{14}$$

which allows determining the fluid evolution either during the compression or the expansion process.

Combustion

Ten chemical species [32, 33] and two regions have been considered inside the chamber (unburned and burned gas regions) for the combustion process. The corresponding chemical reaction is

$$\varepsilon\phi\left(\upsilon_1 CH_4+\upsilon_2 H_2\right)+\left(0.21O_2+0.79N_2+\tilde{\omega}H_2O\right)\rightarrow \mu_1 CO_2+\mu_2 H_2O+\mu_3 N_2+\mu_4 O_2+ \\ +\mu_5 CO+\mu_6 H_2+\mu_7 H+\mu_8 O+\mu_9 OH+\mu_{10} NO \tag{15}$$

The mole amount of product i (i = 1...10) per mole of fuel mixture is represented by μ_i.

To solve this problem, a non-linear equations system constituted by the mass balances

$$\begin{aligned} &C \rightarrow \varepsilon\phi\upsilon_1 = (y_1+y_5)N \\ &H \rightarrow \varepsilon\phi\left(4\upsilon_1+2\upsilon_2\right)+2\tilde{\omega} = \left(2y_2+2y_6+y_7+y_9\right)N \\ &O \rightarrow 0.42+\tilde{\omega} = (2y_1+y_2+2y_4+y_5+y_8+y_9+y_{10})N \\ &N \rightarrow 0.79\cdot 2 = \left(2y_3+y_{10}\right)N \end{aligned} \tag{16}$$

and the equilibrium constants K_p corresponding to dissociation of the products in equilibrium, is available

$$\begin{aligned} &\frac{1}{2}H_2 \rightleftharpoons H && \rightarrow && K_1=\frac{y_7 p^{1/2}}{y_6^{1/2}} \\ &\frac{1}{2}O_2 \rightleftharpoons O && \rightarrow && K_2=\frac{y_8 p^{1/2}}{y_4^{1/2}} \\ &\frac{1}{2}H_2+\frac{1}{2}O_2 \rightleftharpoons OH && \rightarrow && K_3=\frac{y_9}{y_4^{1/2}y_6^{1/2}} \\ &\frac{1}{2}O_2+\frac{1}{2}N_2 \rightleftharpoons NO && \rightarrow && K_4=\frac{y_{10}}{y_4^{1/2}y_3^{1/2}} \\ &H_2+\frac{1}{2}O_2 \rightleftharpoons H_2O && \rightarrow && K_5=\frac{y_7}{y_4^{1/2}y_6 p^{1/2}} \\ &CO+\frac{1}{2}O_2 \rightleftharpoons CO_2 && \rightarrow && K_6=\frac{y_1}{y_4^{1/2}y_5 p^{1/2}} \end{aligned} \tag{17}$$

being y_i the mole fraction of the i species in the products and N the total mole amount of products. Then $\mu_i = y_i.N$ and

$$\sum_{i=1}^{10} y_i = 1 \tag{18}$$

It must be noted that when pure hydrogen is used, $\nu_1 = 0$, $y_1 = 0$, $y_5 = 0$ and K_6 does not apply because carbon is not present in the medium.

The equilibrium constant values are calculated by means of the expression [34]

$$\log K_p = A \ln \frac{T}{1000} + \frac{B}{T} + C + DT + ET^2 \tag{19}$$

with constants A, B, C, D and E being taken from [33, 34].

In addition, the First Law of Thermodynamics is used. As two regions are assumed inside the combustion chamber (unburned and burned gas ones), this equation can be written as

$$Q_u + Q_b - \int_1^2 pdV = \left[U_u + U_b\right]_2 - \left[U_u + U_b\right]_1 \tag{20}$$

where *1* and *2* represent the initial and final states at each calculation step, respectively. Taking into account equation (7), in this case

$$Q_u = \frac{A_u h_u (T_u - T_{w,u})}{n} \Delta\theta \tag{21}$$

$$Q_b = \frac{A_b h_b (T_b - T_{w,b})}{n} \Delta\theta \tag{22}$$

where $\Delta\theta$ is the crank angle increment and

$$\int_1^2 pdV = \frac{p_2 + p_1}{2}(V_2 - V_1) \tag{23}$$

as well as the unburned and burned gas equations of state, the following equation is obtained

$$\left[\frac{A_u h_u \left(\frac{pV_u}{n_u R} - T_{w,u}\right)}{n} + \frac{A_b h_b \left(\frac{pV_b}{n_b R} - T_{w,b}\right)}{n}\right] \Delta\theta - \frac{p_2 + p_1}{2}(V_2 - V_1) = (m_u u_u)_2 - (m_u u_u)_1 - (m_b u_b)_2 - (m_b u_b)_1 \tag{24}$$

where u means specific internal energy.

Similarly to the compression process, the Woschni expression, equations (11) and (12) and Table 1, is used to calculate the heat transfer coefficient, and the Muller expression [31], equation (13), is used to calculate the cylinder wall temperature.

To calculate the volumes occupied by both unburned and burned gas, the mass inside the cylinder is considered to stay constant. In addition, the Livengooz hypothesis [35] is used for the unburned gas

$$pV_u^{\gamma_u} = p_{initial} V_{initial}^{\gamma_u} \tag{25}$$

where $p_{initial}$ and $V_{initial}$ represent the starting combustion pressure and volume, respectively.

Then

$$V_b = V - (1-x)V_{initial}\left(\frac{p_{initial}}{p}\right)^{\frac{1}{\gamma_u}} \tag{26}$$

$$V_u = V - V_b \tag{27}$$

The burned mass fraction x is evaluated by integrating the Vibe [36] function

$$\frac{dx}{d\theta} = \frac{\theta}{\Delta\theta_c}(m+1)\, y^m \exp^{-ay^{(m+1)}} \tag{28}$$

being $\Delta\theta_c$ the combustion development angle. Therefore

$$x = \int \frac{dx}{d\theta} d\theta = 1 - \exp^{-ay^{(m+1)}} \tag{29}$$

being m the shape parameter ($m = 2$) and a stands for the Vibe parameter ($a = 5$).

The expressions used to evaluate the unburned A_u and burned A_b gas wet chamber surface areas are the following

$$A_u = (1-x)\, A \tag{30}$$

$$A_b = x\, A \tag{31}$$

Knock

Knock is an important effect to be taken into account in poly-fuel engines. Appearance of knock has been determined by using empirical models to calculate the induction time τ_{i0}. This is calculated from pure methane and hydrogen induction times by means of the following expression [37]

$$\tau_{i0} = \tau_{CH_4}^{1-\beta} \cdot \tau_{H_2}^{\beta} \tag{32}$$

being

$$\tau = A \cdot \left(\frac{p}{T}\right)^n \cdot \exp\left(\frac{E_a}{RT}\right) \tag{33}$$

where p, T and β are pressure, temperature and the hydrogen molar fraction in the mixture, respectively. Values of parameters A, n and E_a, depending on the fuel, are shown in Table 2.

Table 2. Coefficients for the equation (34)

	A	E_a	n
H_2	2.82E-13	336	-1.3
CH_4	3.23E-2	192	-2.1

Therefore

$$\tau_{i0} = A_{H_2}^{\beta} \cdot A_{CH_4}^{(1-\beta)} \cdot \left(\frac{p}{T}\right)^{n_{H_2}\beta + n_{CH_4}(1-\beta)} \cdot \exp\left(\frac{E_{H_2}\beta + E_{CH_4}(1-\beta)}{RT}\right) \tag{34}$$

Knock appears when the following condition is attained

$$\int_0^t \frac{1}{\tau_{i0}(t)} dt = 1 \tag{35}$$

VALIDATION OF THE MODEL

Experimental results given in [3], obtained under given operating conditions, have been used to validate the model. Therefore, operating conditions imposed in [3] have been used (they can be found in Table 4 of this reference); the experimental results used for validation purposes are shown in Figure 8 of the same reference, and specifications of the engine used in [3] are detailed in [38] and [3]. Thus, specifications of the engine simulated in this work are compiled in Table 3, and the different operating conditions used to validate the model are shown in Table 4, where θ_{ig} represents the spark timing crank angle and ϕ stands for the fuel/air equivalence ratio.

Table 3. Engine specifications

Item	Value
Displacement Volume (cm^3)	1039
Compression Ratio	10.5
Bore (mm)	105
Stroke (mm)	120
Rating Power (kW)	154
Rating Torque (Nm)	620
Intake Valve Open (°BTDC)	18
Intake Valve Close (°ATDC)	37
Exhaust Valve Open (°BBDC)	56
Exhaust Valve Close (°ATDC)	11
Ratio of connecting rod length to crank radius	1.833
Relative offset	0.0422

Table 4. Engine operating conditions

Case	n (rpm)	p_i (bar)	%H_2	ϕ	θ_{ig} (°)
A	1600	0.70	20	0.769	26
B	1600	1.20	20	0.769	26
C	1200	1.05	10	0.752	30
D	1200	1.05	30	0.714	30
E	1600	0.87	40	0.833	24
F	1600	0.65	50	0.800	22
G	2400	0.80	0	0.769	32
H	1200	1.05	0	0.613	30

Figures 5 to 8 show the evolution of the pressure as a function of the crank angle for both experimental and calculated data, in each case. There are two main error sources in cases A to G: some parameters of the actual engine are unknown and have been adjusted to obtain the best approximation and blow-by effect. In case H, the difference between experimental and calculated data is bigger. As shown in Table 4, this case corresponds to pure natural gas and the fuel/air equivalence ratio is 0.613, very close to the lowest operating limit, being the combustion unstable and incomplete. This is not taken into account by the model. In cases A to G the model fits the experimental pressure data with an error lower than 3%.

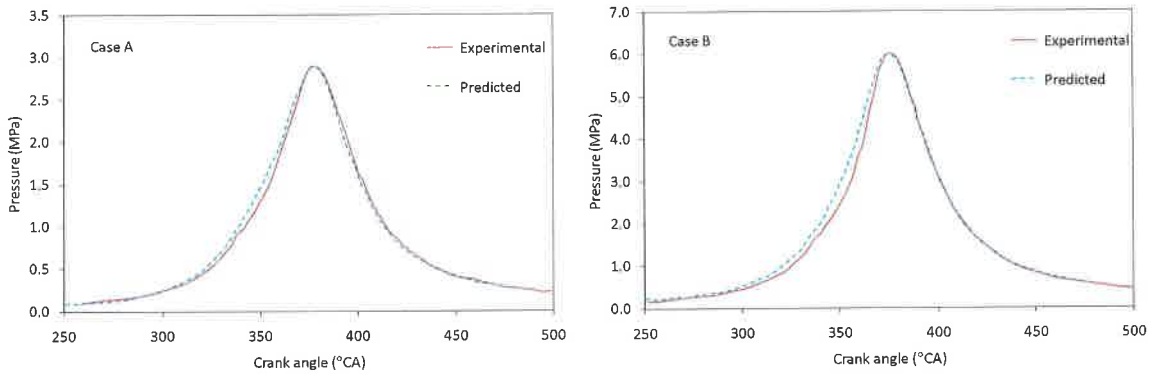

Figure 5. Indicated cycle obtained with the model compared with experimental [3] measurement (cases A and B)

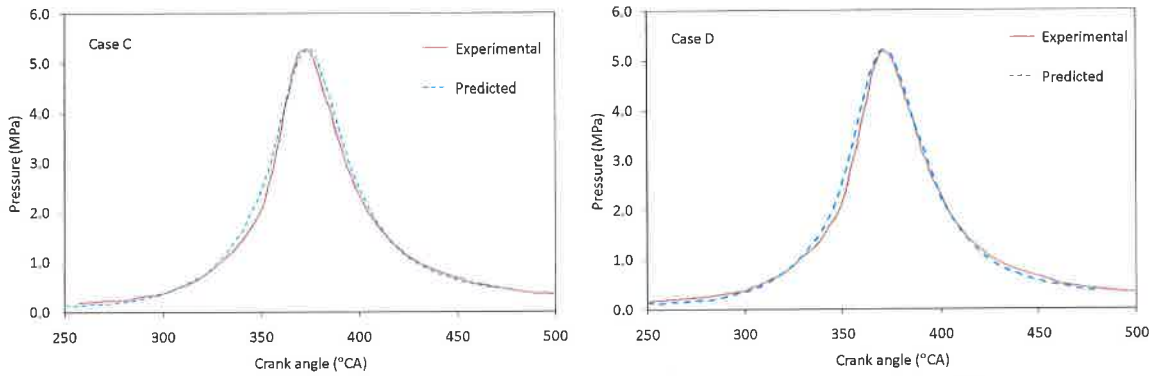

Figure 6. Indicated cycle obtained with the model compared with experimental [3] measurement (cases C and D)

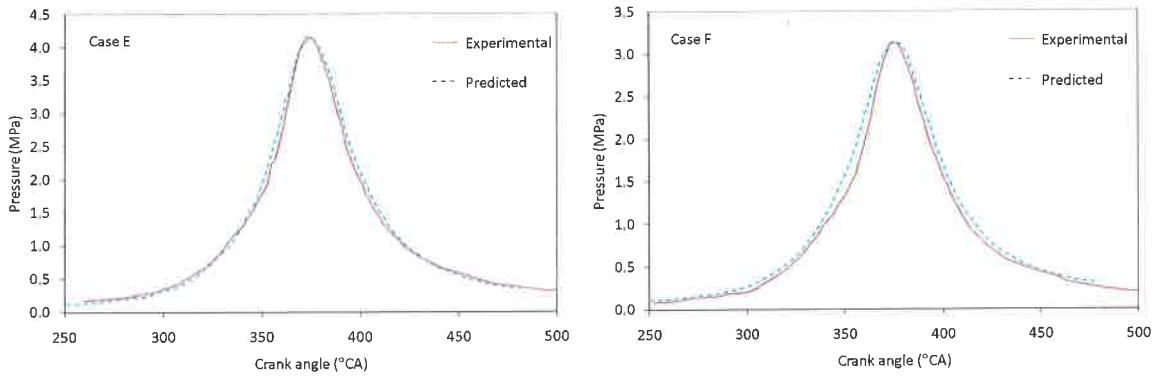

Figure 7. Indicated cycle obtained with the model compared with experimental [3] measurement (cases E and F)

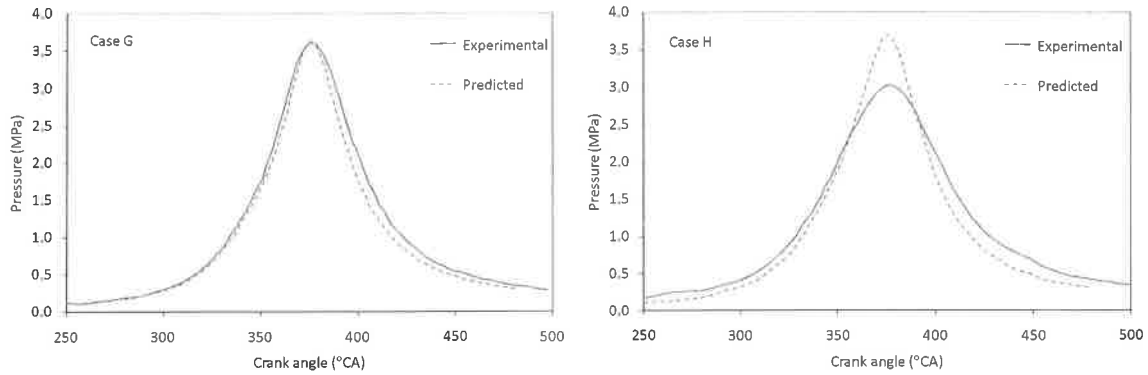

Figure 8. Indicated cycle obtained with the model compared with experimental [3] measurement (cases G and H)

RESULTS AND DISCUSSION

Effect of hydrogen addition on engine performance

In order to evaluate the influence of the hydrogen fraction on engine performance, different fuels are used to run the model. Specifications of the simulated engine are collected in Table 3 and operating conditions can be seen in Table 5.

Table 5. Engine operating conditions

Item	Value
Ambient temperature (K)	294.15
Fuel temperature (K)	294.15
Intake pressure (bar)	0.8
Exhaust pressure (bar)	1.0
Fuel/air equivalence ratio	0.833
Spark timing (°)	17
Speed engine (rpm)	2000

Figure 9 shows the variation of pressure with the crank angle for three mixtures (pure natural gas, HCNG with 50% hydrogen, and pure hydrogen) and different values of the spark timing; Figure 10 shows the indicated work as a function of the spark timing; Figure 11 shows the variation of pressure with the crank angle for the three mixtures and different values of the compression ratio, and Figure 12 represents the power delivered by each fuel as a function of the crankshaft engine rotational speed.

As shown in Figures 9 and 10, the maximum pressure in the cylinder and the indicated work increase as the hydrogen fraction increase. The maximum pressure increases by 8% from pure hydrogen to pure CNG. Consequently, the indicated work and the power delivered are also enhanced with increasing hydrogen amounts. The indicated work increases by a 15.2% from pure hydrogen to pure CNG. This occurs because hydrogen specific energy is higher than that of natural gas. Therefore the temperature reached in the cylinder is also higher. As observed in Figure 9 the crank angle at which the maximum pressure occurs is different for each fuel.

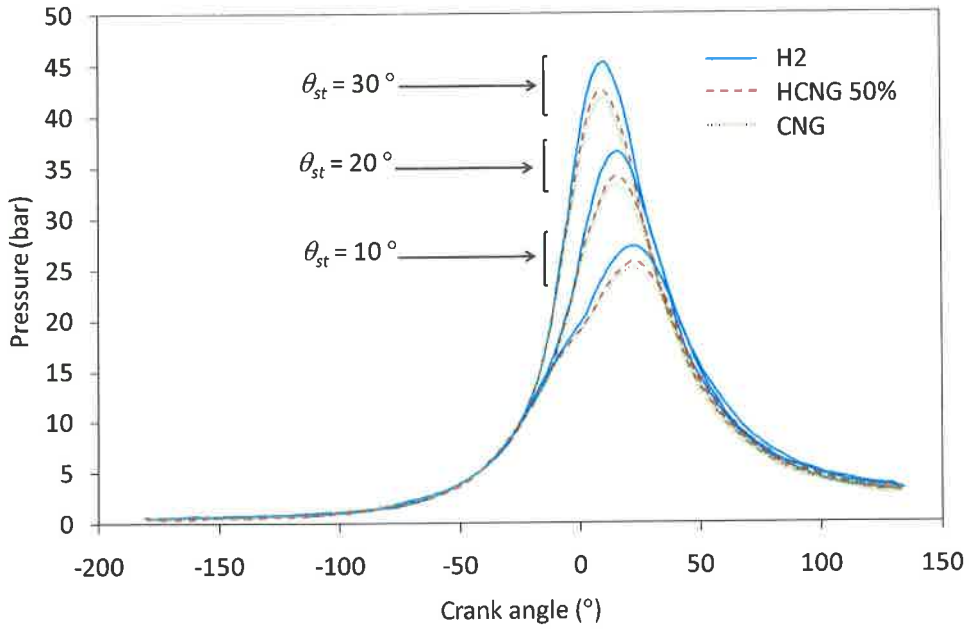

Figure 9. Variation of pressure as a function of the crank angle, fuel composition and spark timing

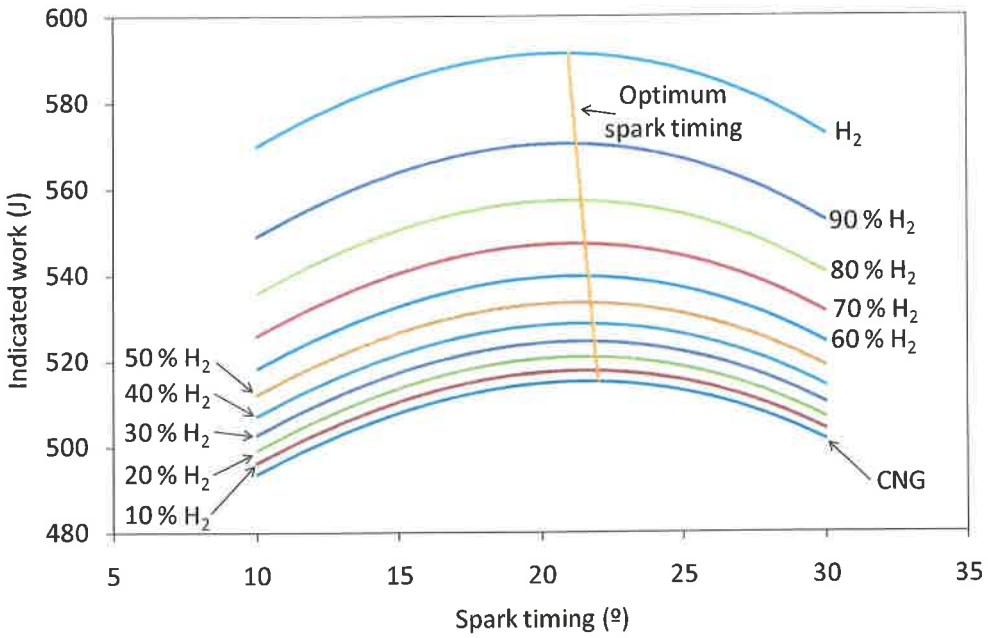

Figure 10. Indicated work as a function of the spark timing and fuel composition

Figure 10 shows the optimum spark timing required to attain the maximum work depending on the hydrogen content in the mixture.

A similar behaviour to that previously indicated is found at two different compression ratios, see Figure 11. The maximum pressure increases as the hydrogen content in the mixture increases. An analogous trend is observed for the power delivered as a function of the engine speed, Figure 12. Similarly to what happens with the indicated work, the power increase is as much higher as higher the hydrogen content is.

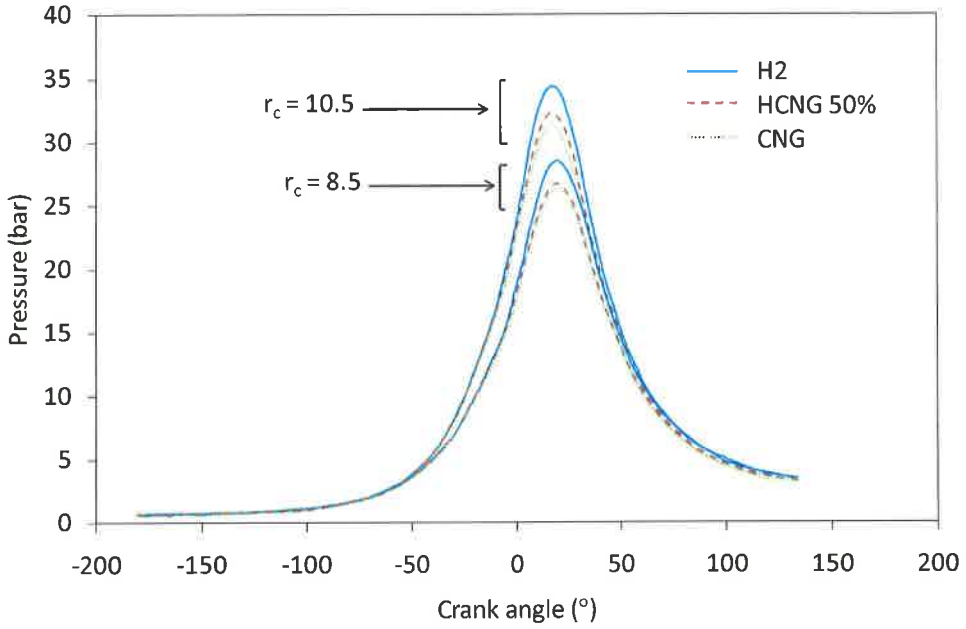

Figure 11. Variation of pressure as a function of the crank angle, fuel composition and compression ratio

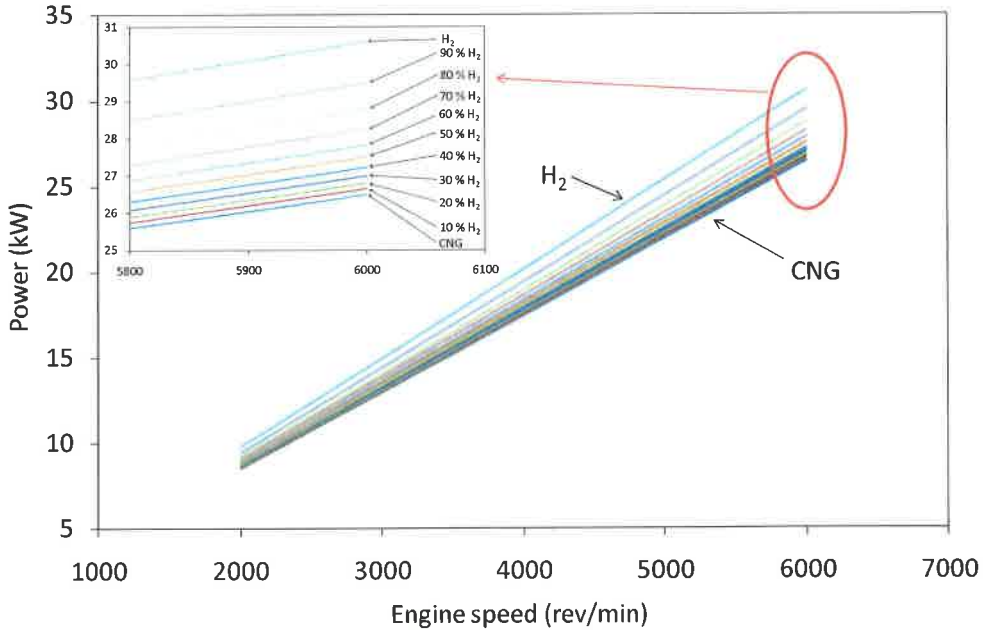

Figure 12. Power delivered by the engine as a function of the crankshaft rotational speed and fuel composition

Figures 13 and 14 show the power delivered as a function of both the intake pressure and the crank angle for natural gas and hydrogen, respectively. Similar results are obtained in both cases: the higher the hydrogen percentage is, the higher are the power results, at equal intake pressure and crank angle values.

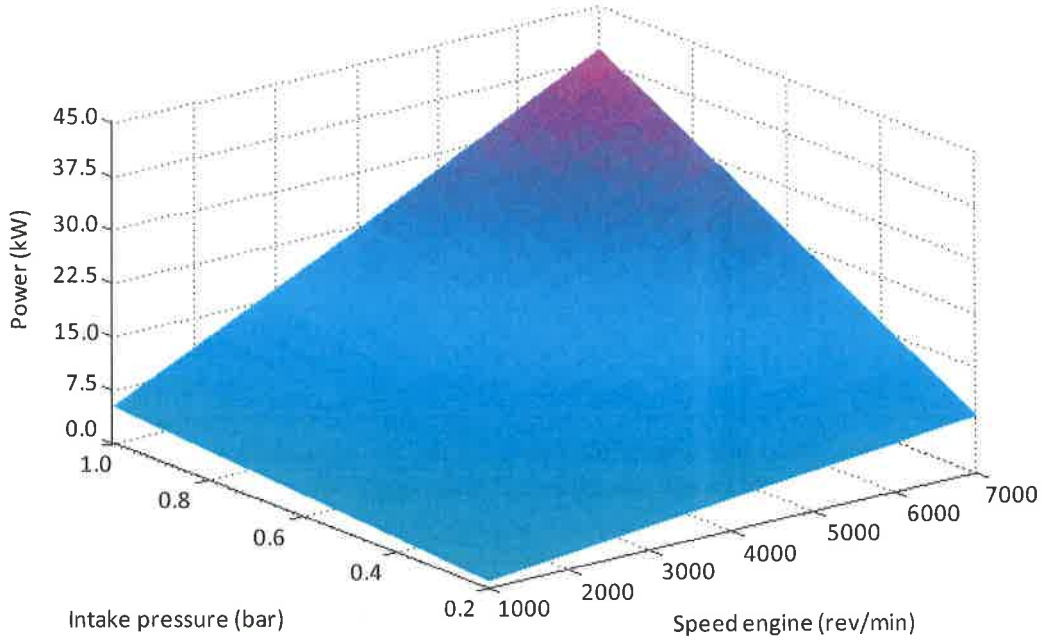

Figure 13. Power obtained as a function of both the intake pressure and crank angle for compressed natural gas

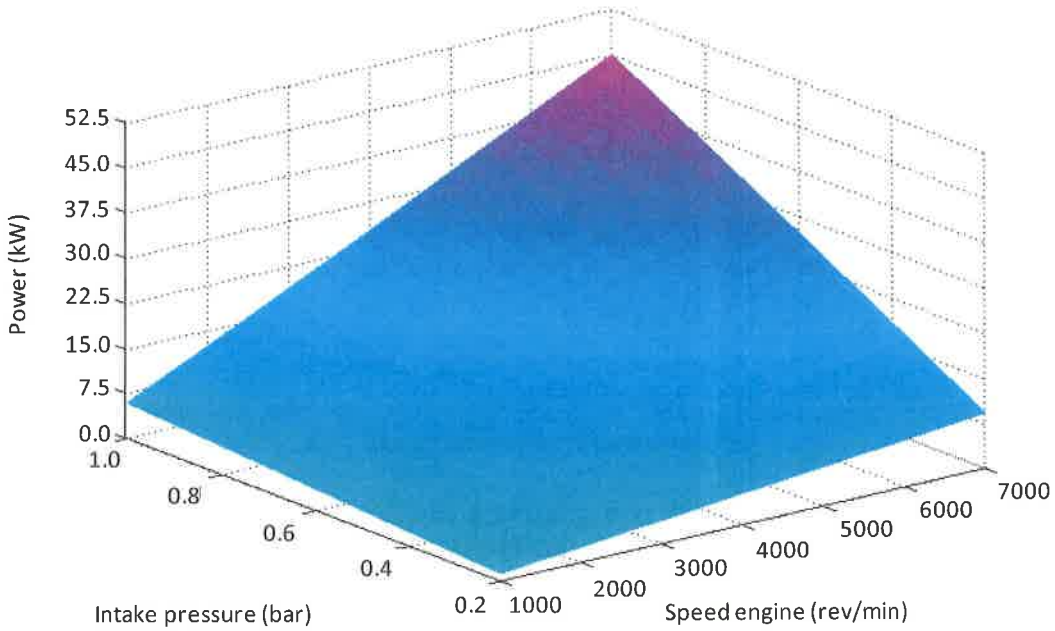

Figure 14. Power obtained as a function of both the intake pressure and crank angle for hydrogen

Effect of hydrogen addition and air/fuel ratio on CO_2 emissions

To analyse the effect of hydrogen addition and the air/fuel ratio on CO_2 emissions, several blends of natural gas and hydrogen have been studied: compressed natural gas, CNG, and HCNG with hydrogen fractions from 10% to 90%, with an air/fuel ratio within reasonable operating limits.

Hydrogen has a high flame propagation speed and a low ignition energy making it possible to work with leaner mixtures than pure natural gas.

There is a limit for lean air-fuel mixtures because if this limit is reached, the combustion becomes unstable and incomplete. Operating close to this limit decreases the combustion speed and increases the ignition energy of the air-fuel mixture, leading to large cycle-by-cycle variations, thus decreasing the thermal efficiency.

Figure 15 shows the CO_2 specific emissions versus the air/fuel ratio for different fuel compositions at three different engine speeds, respectively. As power increases with the engine speed, specific emissions decrease. As an example, for mixtures of 50% and at 2000 rpm, power increases of 9.7% respect to CNG are reached under the studied conditions, and reductions in CO_2 emissions up to 25.9% are attained. It is also observed that emissions decrease with higher amounts of hydrogen and with leaner mixtures. Figure 15 also shows that, as the hydrogen content increases, CO_2 emissions are less affected by the rotational speed.

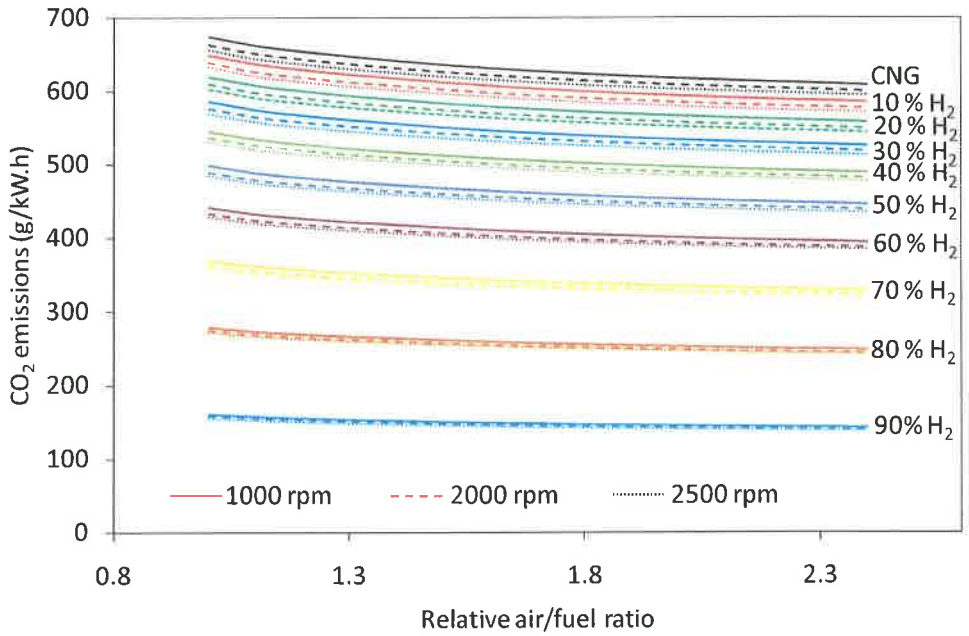

Figure 15. CO_2 emissions as a function of the relative air/fuel ratio, fuel composition and crankshaft rotational speed

It is important to note that both the power increase and the CO_2 decrease show a non linear variation with increasing hydrogen contents, as observed in Figure 16, where the case of relative air/fuel ratio equal to 1.3 has been chosen to be represented. This is an important feature when selecting the optimum hydrogen content in the mixture, because low hydrogen proportions lead to both low CO_2 decreases and power increases. As hydrogen content increases, these phenomena become much more significant. In any case, other factors such as the fuel cost, the required engine's modification cost, the engine's maintenance cost and the safety problems appearing when the H_2 content is increased, must be considered. Therefore, to determine the optimum H_2 proportion in the mixture becomes a complex task, depending on the generation technologies (W-t-W studies) and their cost.

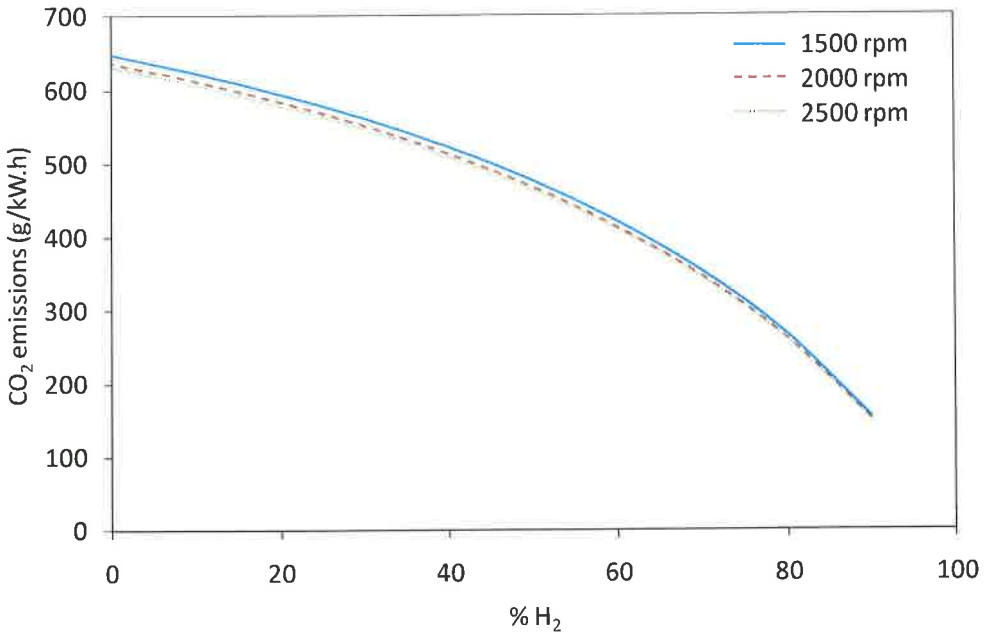

Figure 16. CO_2 emissions as a function of the fuel composition and crankshaft rotational speed (relative air/fuel ratio = 1.3)

CONCLUSIONS

Given the growing importance of alternative fuels, an indicated cycle model for a spark ignition engine operating with variable blends of hydrogen and natural gas (HCNG) has been developed. This model allows modifying geometrical parameters, engine operating conditions and fuel composition. The model has been used to determine the engine's performance and CO_2 emissions and has been previously experimentally validated always giving mean indicated pressure errors under 3%. Maxima cycle pressure and the indicated work obtained increase as the hydrogen proportion in HCNG increases, and leaner mixtures can be used. As the hydrogen content in the mixture increases, CO_2 emissions decrease. Both the CO_2 decrease and the power increase show a nonlinear variation with increasing hydrogen contents, being these phenomena much more significant at high hydrogen contents in the mixture. This, joined to the resulting power increment, makes HCNG be advantageous against other fuels.

ACKNOWLEDGEMENTS

This work has been partially supported by the Universidad Politécnica de Madrid in the frame of the Project Code N° AL11-P(I+D)-03.

NOMENCLATURE

a	crank radius, m; Vibe parameter
A	combustion chamber surface area, m^2; constant for induction time
A_s	throat area
C	constant of Woschni equation
c_D	discharge coefficient
c_p	specific thermal capacity at constant pressure, $J \cdot mol^{-1} \cdot K^{-1}$
C_1	constant of Woschni equation

C_2	constant of Woschni equation
CNG	compressed natural gas
CIG	engine using the Direct Injection Compression Ignition technology (diesel)
D	cylinder bore (m)
e	relative offset (cylinder axis offset from the crankshaft axis/radius of crank)
E_a	constant for induction time
h	specific enthalpy, $J \cdot kg^{-1}$; convection heat-transfer coefficient, $W/m^2 \cdot K$
h_{cc}	equivalent height of combustion chamber, m
HCNG	hydrogen-natural gas blend
H2C	compressed hydrogen
H2L	liquid hydrogen
K_P	equilibrium constant
L	piston strike
LPG	Liquefied Petroleum Gases
m	mass, kg; constant of Woschni equation; shape parameter in Vibe equation
$\dot{m}$	mass flow rate
N	total mole number of products, mol
NG	natural gas
n	crankshaft rotational speed (rad/s, rpm); constant for induction time
p	pressure, kPa
p_m	motored cylinder pressure
p_r	inlet valve closing pressure
p_s	pressure at the throat
p_t	stagnation pressure
Q	heat transfer, J
$\dot{Q}$	heat transfer rate, W
r_c	compression ratio
R	universal gas constant, $J \cdot mol^{-1} \cdot K^{-1}$
R_g	gas constant, $J \cdot kg^{-1} \cdot K^{-1}$
SICNG	engine using the Port Injection Spark Ignition technology (natural gas)
SICNGBF	engine using the Port Injection Spark Ignition technology (gasoline-natural gas)
SID	engine using the Direct Injection Spark Ignition technology (gasoline)
SIH2C	engine using the Port Injection Spark Ignition technology (compressed hydrogen)
SIH2L	engine using the Port Injection Spark Ignition technology (liquid hydrogen)
SILPGBF	engine using the Port Injection Spark Ignition technology (gasoline-LPG)
SIP	engine using the Port Injection Spark Ignition technology (gasoline)
S_P	Mean piston velocity, $m \cdot s^{-1}$
t	time, s
T	temperature, K
T_r	inlet valve closing temperature
T_0	reference temperature, 298.15 K
u	specific internal energy
V	volume, m^3
V_d	displaced cylinder volume
V_r	inlet valve closing volume
x	burned mass fraction

y	instantaneous stroke, m
y_i	mole fraction of species i

Greek letters

β	hydrogen molar fraction in the mixture
ε	total mole number of fuel, mol
γ	thermal capacity ratio c_p/c_v
λ	ratio of connecting rod length to crank radius
ϕ	fuel/air equivalence ratio
η_{vg}	volumetric efficiency
τ	induction time, s
τ_{i0}	induction time, s
θ	crank angle, rad
θ_{ig}	spark timing
$\Delta\theta_c$	combustion development angle
v_i	mole amount of reactant i per mole of fuel mixture
μ_i	mole amount of product i per mole of fuel mixture
$\tilde{\omega}$	molar humidity ratio

Subscripts

b	burned
c	cylinder, cylinder liner
ch	cylinder head
e	exit, exhaust
f	fuel
i	inlet; intake
p	piston crown
u	unburned
w	wall

REFERENCES

1. "*BP Statistical Review of World Energy*", 2010. (http://www.bp.com/liveassets/bp_internet/globalbp/globalbp_uk_english/reports_and_publications/statistical_energy_review_2011/STAGING/local_assets/spreadsheets/statistical_review_of_world_energy_full_report_2011.xls) [accessed June 2011].
2. U.S. Department of Energy "*Transportation Energy Data Book*". (http://cta.ornl.gov/data/tedb29/Edition29_Chapter01.pdf) [accessed June 2011].
3. Fanhua, M., Yu, W., Mingyue, W., Haiquan, L., Junjun, W., Shangfen, D., Shuli, Z., Development and validation of a quasi-dimensional combustion model for SI engines fuelled by HCNG with variable hydrogen fractions, *Int. J. Hydrogen Energy*, Vol. 33, No. 18, pp 4863-4875, 2008.
4. Park, J., Cha, H., Song, S., Chun, K., M., A numerical study of a methane-fuelled gas engine generator with addition of hydrogen using cycle simulation and DOE method, *Int. J. Hydrogen Energy*, Vol. 36, No. 8, pp 5153-5162, 2011.

5. Dimopoulos, P., Rechsteiner, C., Soltic, P., Laemmle, C., Boulouchos, K., Increase of passenger car engine efficiency with low engine-out emissions using hydrogen–natural gas mixtures: A thermodynamic analysis, *Int. J. Hydrogen Energy*, Vol. 32, No. 14, pp 3073-3083, 2007.
6. Bysveen, M., Engine characteristics of emissions and performance using mixtures of natural gas and hydrogen, *Energy*, Vol. 32, No. 4, pp 482-489, 2007.
7. Perini F, Fabrizio Paltrinieri, Enrico Mattarelli, A quasi-dimensional combustion model for performance and emissions of SI engines running on hydrogen-methane blends, *Int. J. Hydrogen Energy*, Vol. 35, No. 10, pp 4687-4701, 2010.
8. Fanhua, M., Mingyue, W., Long, J., Jiao, D., Renzhe, C., Nashay, N., Shuli, Z., Performance and emission characteristics of a turbocharged spark-ignition hydrogen-enriched compressed natural gas engine under wide open throttle operating conditions, *Int. J. Hydrogen Energy*, Vol. 35, No. 22, pp 12502-12509, 2010.
9. Dimopoulos, P., Bach, C., Soltic, P., Boulouchos, K., Hydrogen-natural gas blends fuelling passenger car engines: Combustion, emissions and well-to-wheels assessment, *Int. J. Hydrogen Energy*, Vol. 33, No. 23, pp 7224-7236, 2008.
10. Park, C., Kim, C., Choi, Y., Won, S., Moriyoshi, Y., The influences of hydrogen on the performance and emission characteristics of a heavy duty natural gas engine, *Int. J. Hydrogen Energy*, Vol. 36, No. 5, pp 3739-3745, 2011.
11. Hu, E., Huang, Z., Liu, B., Zheng, J., Gu, X., Huang, B., Experimental investigation on performance and emissions of a spark-ignition engine fuelled with natural gas-hydrogen blends combined with EGR, *Int. J. Hydrogen Energy*, Vol. 34, No. 1, pp 528-539, 2009.
12. Xu, J., Zhang, X., Liu,J., Fan, L., Experimental study of a single-cylinder engine fueled with natural gas–hydrogen mixtures, *Int. J. Hydrogen Energy*, Vol. 35, No. 7, pp 1-6, 2009.
13. Ceper, B. A., Akansu, S. O., Kahraman, N., Investigation of cylinder pressure for H2/CH4 mixtures at different loads, *Int. J.Hydrogen Energy*, Vol. 34, No. 11, pp 4855-4861, 2009.
14. Kahraman N., Ceper, B., Akansu, S. O., Aydi, K., Investigation of combustion characteristics and emissions in a spark ignition engine fuelled with natural gas-hydrogen blends, *Int. J. Hydrogen Energy*, Vol. 34, No. 2, pp 1026-1034, 2009.
15. Akansu, S. O., Bayrak, M., Experimental study on a spark ignition engine fuelled by CH_4/H_2 (70/30) and LPG, *Int. J. Hydrogen Energy*, Vol. 36, No. 15, pp 9260-9266, 2011.
16. IANGV, International Association for Natural Gas Vehicles. (http://www.iangv.org/stats/NGV_Statistics10_files/sheet007.htm#RANGE!A1) [accessed June 2011].
17. Concawe/Eucar/JRC, Well-To-Wheels analysis of future automotive fuels and powertrains in the European context, Report 2007. (http://ies.jrc.ec.europa.eu/uploads/media/WTW_Report_010307.pdf) [accessed June 2011].
18. General Motors Corporation, Well-To-Wheels Analysis of Advanced Fuel/Vehicle Systems – A North American Study of Energy Use, Greenhouse Gas Emissions, and Criteria Pollutant Emissions, 2005. (http://www.transportation.anl.gov/pdfs/TA/339.pdf) [accessed June 2011].
19. Blizard, N. C., Keck, J. C., Experimental and theoretical investigation of turbulent burning model for internal combustion engines. SAE Paper 740191, 1974.
20. Bayraktar H. Theoretical investigation of using ethanol-gasoline blends on SI engine combustion and performance, *Ph. D. Thesis*, Karadeniz Technical University, Trabzon, Turkey, 1997.
21. Bayraktar, H., Theoretical investigation of flame propagation process in an SI engine running on gasoline-ethanol blends, *Renewable Energy*, Vol. 32, No. 5, pp 758-771, 2007.
22. Kang, K., Spng, N.W., Cycle Simulation for a Spark Ignition Engine Using a Turbulent Combustion Model, SAE Paper 872154, 1987.

23. Bascunana, J.L., Burning Rate Development in a Closed Vessel of Arbitraty Shape and Variable Volume, for Variable but Uniform Pressure, *Trans. ASME J. Eng. Power*, Vol. 91A, pp 69-71, 1969.
24. Gatowski, A., Balles, E.N., Chun, K.M., Nelson, F.E., Ekchian, J.A., Heywood, J.B., Heat Release Analysis of Engine Pressure Data, SAE Paper 841359, 1984.
25. Verhelst, S., Sheppard, C.G.W., Multi-zone thermodynamic modelling of spark-ignition engine combustion – An overview, *Energy Conversion and Management*, Vol. 50, No. 5, pp 1326-1335, 2009.
26. Caton, J.A., Implications of fuel selection for an SI engine: Results from the first and second laws of thermodynamics, *Fuel*, Vol. 89, No. 11, pp 3157-3166, 2010.
27. Navarro, E., Varela, E., Descomposición en serie de la presión generada por la combustión en Motores Alternativos, *Anales de Ingeniería Mecánica*, Vol. 9, pp 45-49,1992 (ISSN: 0212-5072).
28. Kempinski, J.M., Knock in Spark Ignition Engines, SAE paper 810147, 1981.
29. Poling, B.E., Prausnitz, J.M., O'Connell, J.P., *The Properties of gases and Liquids*, 5 ed., McGraw-Hill, New York, 2001.
30. Woschni, G., A Universal Applicable Equation for the Instantaneous Heat Transfer Coefficient in the Internal Combustion Engine, SAE paper 670931, 1967.
31. Müller, H., Bertling, H., *Programmierte Auswertung von Druckverläufen in Ottomotoren*, VDI-Verlag, Düsseldorf, 1971.
32. Svehla, R.A., McBride, B.H., *Fortran IV Computer Program for Calculation of Thermodynamics and Transport Properties of Complex Chemical Systems*, NASA TN D-7056, 1973.
33. Ferguson, C.R., *Internal Combustion Engines: Applied Thermosciences*, John Wiley & Sons, New York, 1986.
34. Olikara, C., Borman, G.L., A Computer Program for Calculating Properties of Equilibrium Combustion Products with Some Applications to I.C. Engines, SAE paper 750468, 1975.
35. Livengood, J.C., Taylor, C.F., Wu, P.C., Measurement of Gas Temperature in an Engine by the Velocity of Sound Method, SAE paper 580064, 1958.
36. Vibe, I.I., *Brennverlauf und Kreisprozess von Verbrennungsmotoren*, Verlag Technik, Berlin, 1970.
37. Gersen, S., Experimental study of the combustion properties of methane/hydrogen mixtures, *M. Sc. Thesis*, University of Groningen, 2007.
38. Fanhua, M. A., Yu, W., Haiquan, L., Yong, L., Junjun, W., Shangfen, D., Effects of hydrogen addition on cycle-by-cycle variations in a lean burn natural gas spark-ignition engine, *Int. J. Hydrogen Energy*, Vol. 33, No. 2, pp 823-831, 2008.